



# Study of lithium diffusion in RF sputtered Nickel–Vanadium mixed oxides thin films

F. Artuso<sup>a,\*</sup>, F. Bonino<sup>a</sup>, F. Decker<sup>a</sup>, A. Lourenco<sup>b</sup>, E. Masetti<sup>c</sup>

<sup>a</sup> Chemistry Department, 'Istituto Nazionale di Fisica della Materia', University of Roma 'La Sapienza', I-00185 Roma, Italy

<sup>b</sup> Instituto de Fisica, University of Campinas, São Paulo, Brazil

<sup>c</sup> ENEA-C.R. Casaccia, Via Anguillarese 301, I-00060 Roma, Italy

Received 22 June 2001; received in revised form 29 September 2001

## Abstract

The kinetics of electrochemical lithium insertion inside RF sputtered Ni/V mixed oxides thin films have been investigated employing different electrochemical techniques. The AC electrochemical impedance spectra, recorded after 10 cycles, showed three steps clearly involved in the intercalation mechanism of lithium in the oxide films: (i) a charge transfer process to the electrolyte/electrode interface; (ii) a solid-state diffusion of Li; and (iii) a space limited diffusion due to the finite volume of the film. This latter portion of the impedance spectra was used to calculate the Li chemical diffusion coefficients ( $D_{Li}$ ).  $D_{Li}$  values show an initial increase up to an injected charge of  $30 \text{ mC cm}^{-2}$  and then, upon further intercalation, a decay probably due to the limited Li motion through a decreased number of available sites. These results are in good agreement with the ones obtained by potentiostatic intermittent titration technique applied to the same electrodes. Both techniques agree in giving the same trend for  $D_{Li}$  upon Li intercalation. The same sets of measurements were carried out after 100 and 1000 Li insertion/deinsertion cycles in order to analyze the effect of prolonged cycling on the mechanism of lithium diffusion. © 2002 Elsevier Science Ltd. All rights reserved.

**Keywords:** Lithium diffusion; EIS; PITT

## 1. Introduction

Transparent polymer [1] or oxide [2] thin films with mixed (ionic–electronic) conductivity have been studied for ion-intercalation reactions in electrochromic devices (ECDs). Due to insufficient cycling stability of polymers compared with inorganic systems, most transparent electrodes used for ECDs are transition metal oxide films.

The class of vanadates is particularly suitable for such kind of electrochemical devices [2–4] because of their layered structure that allows an easy insertion/extraction of different ions between its slabs. The intercalation/deintercalation process is the basis for device operation because color changes in the electrodes are associated with the concentration changes of the inserted ion charge.

In the field of ECDs, transition metal vanadates in form of thin films have given rise to considerable interest as ion-storage layers when used together with  $\text{WO}_3$ , which is usually the optically active EC electrode [2]. Promising results have been achieved in our laboratories with RF sputtered thin films of Ce/V and Ni/V mixed oxides [5,6]. These materials have shown: (i) high charge capacities exceeding  $50 \text{ mC cm}^{-2}$ , largely sufficient to darken the complementary  $\text{WO}_3$  electrode; (ii) good cycling stability which ensures a long device lifetime; and (iii) high transparency both in the intercalated and deintercalated states, to provide with a good optical contrast the variable smart windows. However, in order to obtain a fast device response, an additional requirement has to be satisfied. The film used as counter-electrode must have a fast kinetics of charge insertion/extraction, when compared to the one of  $\text{WO}_3$ . The response time of the device is largely determined by two processes, the interfacial charge transfer and the diffusion of the inserted species. Studies on the kinetics of lithium insertion in RF sputtered Ce/V mixed oxide

\* Corresponding author.

E-mail address: [artuso@uniroma1.it](mailto:artuso@uniroma1.it) (F. Artuso).

films have been previously published by Varsano et al. [7]. The results of their investigations demonstrated the usefulness of using different and complementary electrochemical transient techniques (Potentiostatic Intermittent Titration Technique, PITT, and Galvanostatic Intermittent Titration Technique, GITT) together with Electrochemical Impedance Spectroscopy (EIS) for studying charge transport phenomena and solid-state diffusion of Li inside thin film oxide electrodes. In their work it was shown that the rate of the charge/discharge process was limited by a slow diffusion of lithium in the mixed oxide electrode.

On the basis of these encouraging results we decided to apply the same electrochemical methods to the study of lithium solid-state diffusion in Ni/V RF sputtered films.

The present work aimed to investigate the electrochemical properties of Ni/V mixed oxides thin films and to study the kinetics of Li intercalation process by using and comparing two methods, PITT and EIS. Both transient techniques are useful tools for the kinetics studies of intercalation electrodes. Impedance spectroscopy is of fundamental importance for understanding all the physical phenomena involved during lithium insertion and for quantitatively determining the process of Li diffusion through the films and across the interfaces (high frequency domain). We found out that PITT is more suitable for detecting solid-state diffusion and more accurate for calculating Li chemical diffusion coefficients.

## 2. Experimental

Thin films of Ni/V mixed oxides have been prepared by RF sputtering on substrates of ITO- and B270-glass.

The samples were obtained using as target a pressed powder disc, previously prepared mixing NiO (CERAC) and V<sub>2</sub>O<sub>5</sub> (CERAC) chemicals in a Ni/V atomic ratio of 1:9 and compressing the mixture in a stainless steel holder with 15 cm of diameter at room temperature. The working pressure in the deposition chamber was 30 mTorr, and argon and oxygen partial pressures were in the ratio of 5:1. The RF power applied was 200 W.

The film microstructure was analysed by X-ray diffraction (XRD). The films were found to be amorphous.

The atomic composition and film density were measured by Rutherford Backscattering Spectroscopy (RBS). This analysis confirmed that the Ni/V atomic ratio in the films is the same than in the target. The film density was equal to 3.5 g cm<sup>-3</sup>. The film thickness, measured by optical methods with a Perkin–Elmer  $\lambda$ 9 spectrophotometer, was found to be around 110 nm. Spectrophotometric measurements were also performed

and transmittance and reflectance data have been reported elsewhere [5].

Electrochemical measurements were carried out in three-electrode cells hermetically sealed under Ar atmosphere. Lithium foils were used as counter and reference electrodes and 1.0 M LiClO<sub>4</sub>/PC solution as electrolyte.

To promote Li insertion Cyclic Voltammetry (CV) and chronopotentiometry were accomplished between the potential limits of 1 and 4.5 V versus Li and using an EG&G PAR 273 Potentiostat/Galvanostat. The CV curves were recorded after 10, 100 and 1000 cycles at a scan rate of 20 mV s<sup>-1</sup>. The galvanostatic measurements were carried out after CVs cycles using a constant current density of  $\pm 50 \mu\text{A cm}^{-2}$ .

A frequency response analyser module coupled with a potentiostat/galvanostat Ecochemie Autolab 12 was used to measure the complex electrode impedance, taking an AC modulation amplitude of 10 mV r.m.s. in the frequency range from 50 KHz to 1 MHz. A set of spectra was taken after 10, 100 and 1000 CV cycles. Each spectrum was recorded after injection of 6 or of 12 mC cm<sup>-2</sup> at constant  $I = -20 \mu\text{A cm}^{-2}$  for 300 or 600 s. The open circuit voltage was allowed to relax for 25000 s when the potential variation was  $4 \times 10^{-7}$  V s<sup>-1</sup> or less. The same potentiostat/galvanostat was used for PITT experiments. This technique consists in applying a potential step with small amplitude ( $\sim 5$ –50 mV) and in recording the chronoamperometric response till a uniform intercalant concentration is reached. After the first set of EIS measurements, PITT pulses were recorded continuously from the open circuit voltage 3.4 V down to 1.7 V with potential steps of 25 mV followed by a relaxation time of 1000 s. PITT results after 100 and 1000 cycles were taken after injection of 6 mC cm<sup>-2</sup> at constant  $I = -20 \mu\text{A cm}^{-2}$  for 300 s. The potential steps applied were of 25 and 50 mV after 100 and 1000 cycles, respectively. The relaxation time after each potential step was always 1000 s.

## 3. Results

### 3.1. CV and galvanostatic measurements

Cyclic voltammograms of Ni/V mixed oxide electrodes, within a potential sweep window between 1 and 4.5 V, are reported in Fig. 1. The open circuit voltage of the as-deposited film was 3.6 V. One cathodic peak (B) at 1.7 V with a shoulder around 2.5 V (peak A) was well visible after 10 cycles, but during the anodic scan (extraction) these two steps were not distinctly separated. The positions of the peaks were quite similar to those of V<sub>2</sub>O<sub>5</sub> reported in literature [8] so it could be assumed that only vanadium participate to the redox reaction while nickel was not electrochemically active during the intercalation/deintercalation process as de-

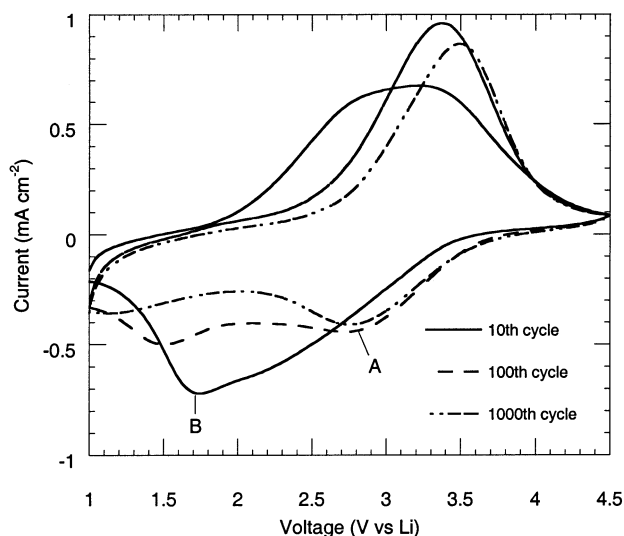


Fig. 1. Cyclic voltammograms recorded at scan rate of  $20 \text{ mV s}^{-1}$  after 10, 100 and 1000 cycles. Electrolyte,  $1 \text{ M LiClO}_4/\text{PC}$ ; lithium reference and counter electrodes. Potential window,  $1.0\text{--}4.5 \text{ V}$  versus Li.

monstrated elsewhere [5]. The charge capacity was as high as  $53 \text{ mC cm}^{-2}$  and the process had already a good reversibility at the 10th cycle. Further cycling up to 20 scans lead to the development of the peak A and to a decreasing in intensity of the second cathodic peak. This splitted feature grew further after 100 cycles when two cathodic peaks appeared distinctly separated at 2.7 and 1.5 V. During the positive scan the single anodic peak became sharper and was displaced to a higher potential (3.4 V). This behavior can be ascribed both to a decrease in the ionic diffusion rate and to an increase of film resistance due to the formation of a passivation layer on the electrode surface. Finally the cyclic voltammogram, taken after 1000 cycles, showed that the cathodic peak B at lower potentials tends to vanish while peak A does not change. The charge capacity of the electrode dropped from 51 (100 cycles) to  $42 \text{ mC cm}^{-2}$ .

Chronopotentiometric results were obtained at a current density of  $\pm 50 \mu\text{A cm}^{-2}$  after 10, 100 and 1000 CV cycles. The curves had a monotonic behavior and did not show any plateau typical of a phase change. This confirmed the amorphous nature of the films. A slight capacity fading occurred with prolonged cycling as the charge capacity passed from  $56 \text{ mC cm}^{-2}$  (10th cycle) down to  $48 \text{ mC cm}^{-2}$  (100th cycle) and to  $44 \text{ mC cm}^{-2}$  (1000th cycle) but the inserted charge was still quite large. Most of the irreversible charge was retained permanently during the first cycles. Nevertheless, the intercalation/deintercalation process kept a high reversibility even after 1000 cycles.

### 3.2. EIS measurements

EIS was used as a tool to investigate, among other properties, the film electrode intercalation kinetics. In

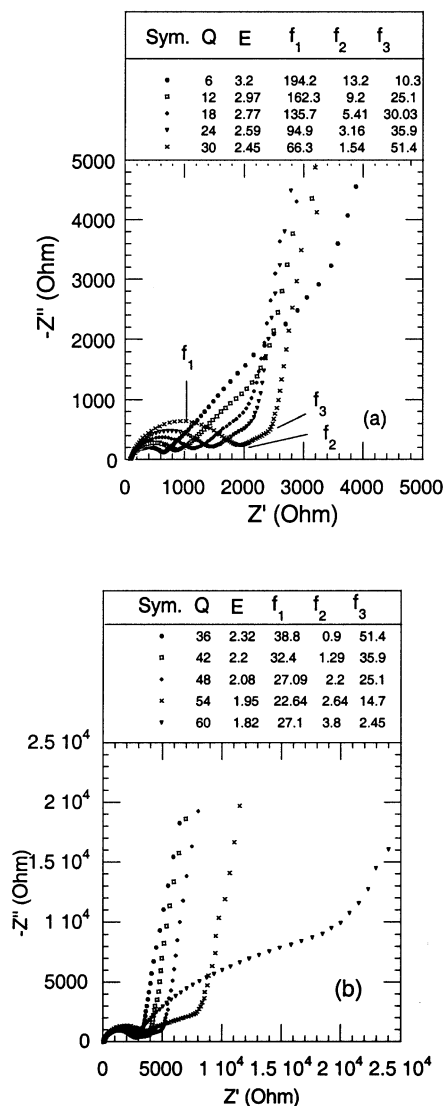


Fig. 2. Nyquist plots of Ni/V mixed oxides recorded after 10 cycles at several inserted charge values (a) from 6 to  $30 \text{ mC cm}^{-2}$ ; (b) from 36 to  $60 \text{ mC cm}^{-2}$ . In the tables are indicated: the inserted charge  $Q$  ( $\text{mC cm}^{-2}$ ); the equilibrated open circuit potential  $E$  (V); the frequencies  $f_1$ ,  $f_2$  (Hz) corresponding respectively to the maximum and the onset of the high frequency loop and  $f_3$  (mHz) the lower frequency of the Warburg region, as shown in the figure.

Fig. 2a and b typical Nyquist plots are reported for films at various intercalation levels (every  $6 \text{ mC cm}^{-2}$ ) after 10 deep charge/discharge cycles. Good separation of the relevant time constants was obtained. The recorded impedance spectra showed three processes clearly involved in the intercalation mechanism of Li in the oxide films: (i) a charge transfer process typical of electrolyte/electrode interface (semicircle at high frequencies); (ii) a solid-state diffusion of Li (straight line at about  $45^\circ$  in the medium frequencies range); and (iii) a space limited diffusion due to the finite volume of the thin film corresponding to a steep, almost vertical line extending to low frequencies. This last feature of the spectra is

typical of intercalation electrodes in form of thin films deposited on electronic conductors impermeable to Li ions (i.e. ITO).

The low frequency part of the spectrum was used to calculate the Li chemical diffusion coefficient according to the following formula reported in literature [9]:

$$D_{\text{Li}} = \frac{Z'' 2\pi\nu l^2}{3R_L} \quad (1)$$

where  $Z''$  is the imaginary part of the impedance at a frequency  $\nu$ ,  $R_L$ , limiting resistance and  $l$ , film thickness. Eq. (1) is based on the assumption that diffusion is driven by a gradient in composition and not by an electric field.

As shown in Fig. 3, the limiting resistance was obtained taking into account the abscissa of L ( $Z_L$ ), i.e. of the intersection of the two straight lines fitting the  $45^\circ$  portion of the spectrum and the finite diffusion part at low frequency. The ohmic resistance of the electrolyte plus the electrode  $R_b$ , and the charge transfer resistance  $R_{ct}$  were evaluated by the fitting of the high frequency semicircle using the Boukamp non-linear least-squares program.  $R_L$  was calculated by subtracting  $R_b$  and  $R_{ct}$  to  $Z_L$ . Fig. 3 also shows the equivalent circuit used to simulate the spectra and the corresponding fit of the Nyquist plot obtained after  $6 \text{ mC cm}^{-2}$  of inserted charge. The values resulting from the fit are in good agreement with the experimental data giving a  $\chi^2 = 2.35 \times 10^{-3}$ .

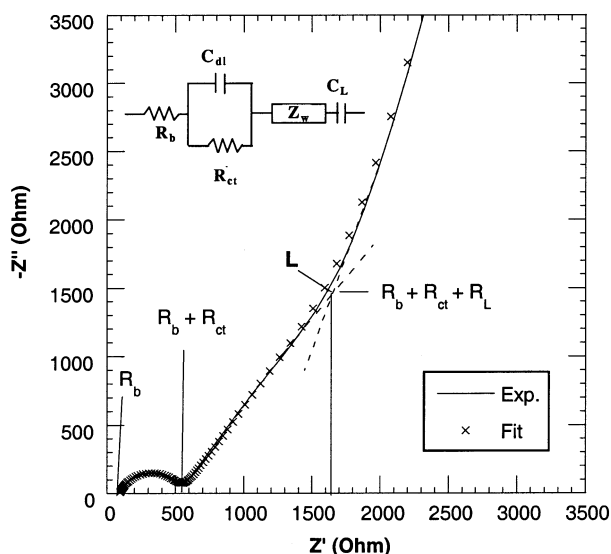


Fig. 3. EIS spectrum of Ni/V mixed oxides taken after 10 cycles with an inserted charge of  $6 \text{ mC cm}^{-2}$ .  $R_b$  indicates the ohmic resistance of electrolyte and electrode and  $R_{ct}$  is the charge transfer resistance. The limiting resistance  $R_L$  was calculated subtracting  $R_b$  and  $R_{ct}$  to the real part of point L (intersection between the lines extrapolating the Warburg region and the finite diffusion part). An equivalent circuit used to simulate Nyquist plots and the corresponding data fit for the above mentioned spectrum are also shown.

The space-limited diffusion region of EIS spectra (data points with  $f < f_3$ ) showed a slope slightly below  $90^\circ$  and we used a constant phase element (CPE) to simulate it. This anomalous behavior was already observed by other authors [10] and explained as due to the electrode porosity and to the roughness at the blocking interface electrode/ITO.

Fig. 4 shows the Nyquist plots of the Ni/V film electrode after 100 and 1000 charge/discharge CV cycles, respectively. One can observe that the impedance spectra recorded after 100 cycles display more depressed high frequency semicircles. The spectra at 1000 cycles indicate that upon cycling the total impedance of the electrodes had gradually increased. This was probably due to changes on the electrode surface with formation of passivation layers as it will be discussed in Section 4. A model for fitting these spectra was already proposed by Aurbach et al. [16] and is also shown in Fig. 4. This model includes the same circuit as in Fig. 3, in series with a 'Voight'-type analog (several elements in series, constituted by a resistance and a capacitance  $C$  in parallel  $R||C$ ). These  $R||C$  elements reflect the Li ion insertion through the multilayer surface films. In this case, as the time constants of the different processes overlap, the Warburg region was not clearly distinguishable and we could not calculate  $D_{\text{Li}}$ . For this reason we used PITT as investigation technique to calculate diffusion coefficients with higher accuracy, in particular for aged electrodes.

### 3.3. PITT measurements

A much larger number of data points for  $D_{\text{Li}}$  versus the electrode potential (and thus vs. the intercalation level) has been obtained using PITT, a technique that has been successfully applied for the characterization of Li solid-state diffusion not only in different graphite materials [11–13] but also in other oxide thin film electrochromic samples [7].

The chronoamperometric curve (Fig. 5a) has been analyzed in terms of  $It^{1/2}$  versus  $\log t$  plot (Fig. 5b) according to a procedure established by Levi et al. [14]. This is a convenient way to analyze PITT data because the functional dependence of  $It^{1/2}$  on  $\log t$  reflects different kinetics regions of the entire intercalation process involved during the potentiostatic step. In fact, plotting the time dependence of the product  $It^{1/2}$ , one can clearly distinguish the region in which the current decrease is limited by the diffusion of Li in the oxide matrix. This time domain, called Cottrell region (zone II in Fig. 5b), corresponds in the plot to a plateau characterized by a constant value of  $It^{1/2}$  which is defined by the following equation:

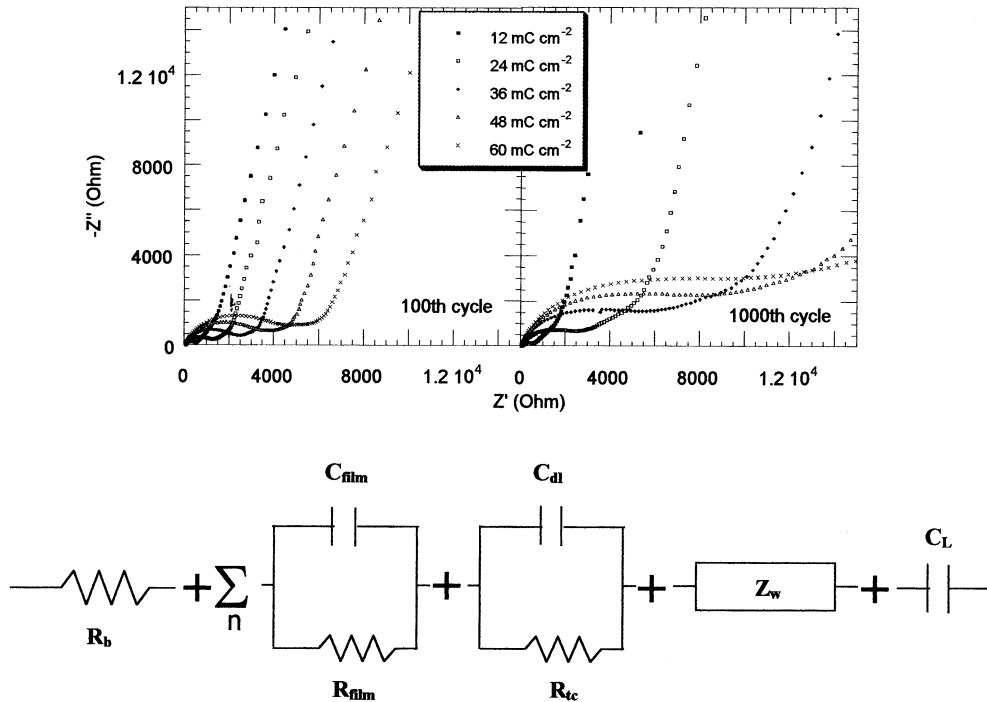


Fig. 4. Nyquist plots of Ni/V mixed oxides recorded at different inserted charges (every  $12 \text{ mC cm}^{-2}$ ) after: 100 cycles, and 1000 cycles. A circuit model for these spectra is also proposed.

$$It^{1/2} = \frac{D_{\text{Li}}^{1/2} \Delta Q}{l\pi^{1/2}} \quad (2)$$

where  $D_{\text{Li}}$  is the chemical diffusion coefficient of Li species inside the film,  $\Delta Q$ , amount of charge inserted during the potentiostatic step and  $l$ , diffusion path length. In this specific case, as we dealt with thin films, it was reasonable to assume  $l$  equal to the film thickness (110 nm). The diffusion coefficients were all calculated by means of Eq. (2).

In Fig. 5b several  $It^{1/2}$  versus  $\log t$  curves are shown, recorded at different potentials after 10 cycles of Li intercalation/deintercalation. Several physical phenomena, corresponding to different time intervals, are evidenced in the bold type plot.

The first zone (I) represents the occurrence of the interfacial charging of the electrode/electrolyte interface. The long-term behavior (zone IV) of the curve describes the finite-space diffusion that is due to accumulation effects at the blocking interface with ITO, and zone III corresponds to a transition region. At long times (region V)  $It^{1/2}$  reaches again a constant value. As indicated by Levi et al. [14] this pseudo-Cottrell behavior is due to the compensation of the decrease in current and a corresponding increase in  $t^{1/2}$  values.

The values of  $It^{1/2}$  in the Cottrell regions II are potential dependent and follow a systematic trend. First the absolute values of the  $It^{1/2}$  plateaux increase as the potential approaches the cathodic peak B in the CV, because current and  $\Delta Q$ , on the basis of Eq. (2), are

getting larger in this region. At lower potentials (and high intercalation level) the values of  $It^{1/2}$  decrease again, with the Cottrell region moving toward longer time. This second feature is related to an increase of the diffusion time once the voltammetric peak B is overcome. In this case the Cottrell region is present only at very long time. The diffusion coefficients calculated from Eq. (2) are shown in Figs. 6 and 7. At the 1000th cycle it was possible to calculate  $D_{\text{Li}}$  only in few points because the Cottrell region was not detectable.

#### 4. Discussion

First qualitative information on the intercalation kinetics and on the ion charge capacity of Ni/V sputtered thin film oxides was obtained from CV and galvanostatic measurements. The CV curves, recorded after various cycles and reported in Fig. 1, revealed the presence of two electrochemically active zones, A and B, thus of two processes mainly occurring during the Li insertion. These two cathodic peaks can be related both to the reduction of vanadium from  $\text{V}^{5+}$  to lower oxidation states or to different insertion mechanisms of lithium in different intercalation sites. After the first 10 CV cycles insertion rate was still slow at high potentials while it was faster in the region between 1.5 and 2 V. With prolonged cycling the current flow in the potential interval between 2.7 and 3.5 V (peak A) increased showing an improving of the intercalation

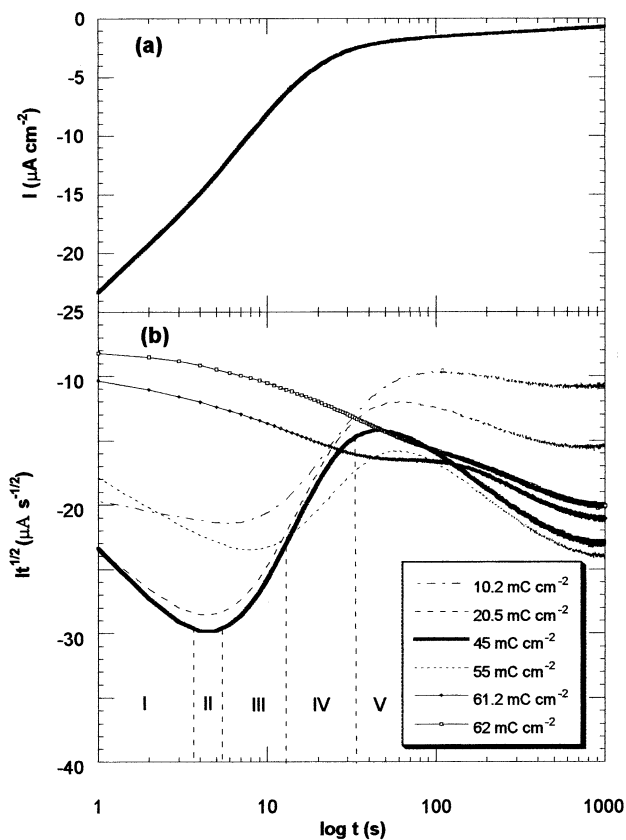


Fig. 5. (a) Typical chronoamperometric response of Li intercalation in Ni/V thin films. The curve is relative to a potential step from 2.130 to 2.105 V; (b)  $It^{1/2}$  versus  $\log t$  representation for Ni/V mixed oxide thin films, from the current relaxation after several potential steps (PITT). The curve in bold corresponds to the same potential step shown in (a). Experiment performed after 10 charge/discharge CV cycles and continuously at growing intercalation levels.

reaction kinetics. The process related to peak B became more irreversible and slower, as this cathodic peak

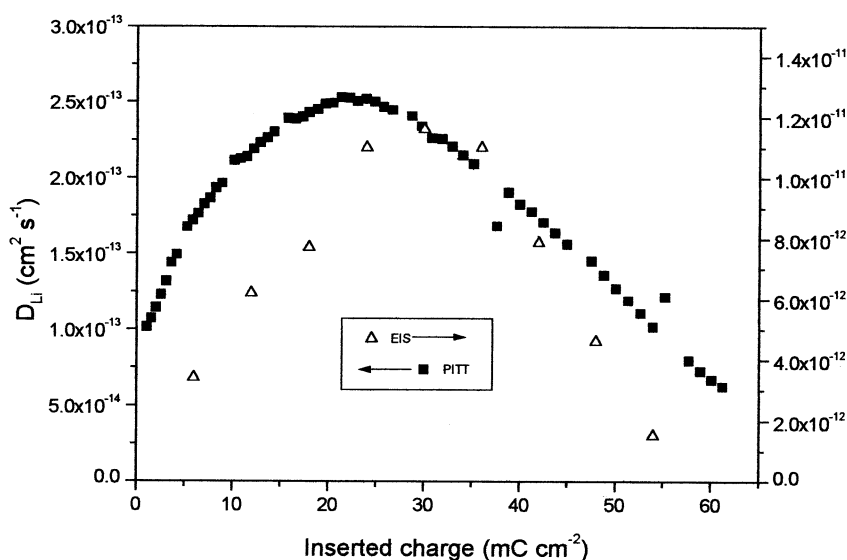


Fig. 6. Diffusion coefficients as a function of the inserted charge calculated, after 10 charge/discharge CVs, from PITT and from EIS.

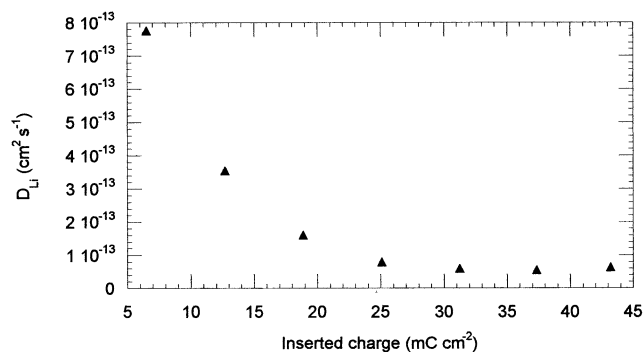


Fig. 7. Diffusion coefficients as a function of the inserted charge calculated from PITT experiments after 100  $\text{Li}^+$  intercalation/deintercalation CV cycles.

moved to lower voltage (around 1.5 V) and tended to vanish with increasing number of cycles.

The modifications of the kinetics properties observed with CV were reflected in the changes of EIS and PITT responses. From AC impedance spectroscopy it was possible to better individuate various factors limiting the intercalation processes. Three main physical phenomena were occurring with Ni/V films after 10 cycles of charge/discharge (Fig. 2a and b) as previously elucidated in the Section 3.2. The enlargement of the high frequency semicircle with the intercalation level indicated that modifications of the surface electrode during Li insertion process lead to an increase of the charge transfer resistance. We can speculate that the dependence of  $R_{ct}$  on the potential was connected with changes of the electronic properties on the surface region. At middle-low frequencies, a Warburg impedance was clearly defined at intercalation levels up to  $36 \text{ mC cm}^{-2}$ . This diffusive element appeared as a straight line segment in the plots, which became shorter and with a lower slope,

the higher the intercalated charge. This behavior could be due to the overlapping of the charge transfer and of the diffusion at lower potentials. Upon an intercalation level of  $60 \text{ mC cm}^{-2}$  the EIS spectrum abruptly changed. The total cell impedance enormously increased and a second semicircle at medium frequencies grew under the Warburg region. The behavior of impedance spectra at such high intercalation levels was not fully interpreted yet.

All  $D_{\text{Li}}$  values were evaluated from EIS results according to Eq. (1).  $D_{\text{Li}}$  versus inserted charge is plotted in Fig. 6, showing an initial increase up to  $1.16 \cdot 10^{-11} \text{ cm}^2 \text{ s}^{-1}$ , for charges less than  $30 \text{ mC cm}^{-2}$ , and thereafter a decay down to  $1.52 \cdot 10^{-12} \text{ cm}^2 \text{ s}^{-1}$  for larger charges. The non-monotonic behavior of  $D_{\text{Li}}$  versus  $Q_{\text{ins}}$  could be associated to the overlapping effect of the two intercalation processes occurring in different hosting sites, as already shown by Deb and coworkers [15] in  $\text{WO}_3$  films. In fact, on the basis of a gas lattice model one would have expected a monotonic decay of  $D_{\text{Li}}$  upon intercalation. However, the slow down of the lithium diffusion rate at high potentials was probably masked by the take-over of a second competing intercalation process occurring in the region B of the CV curve. Once the peak B was overtaken two phenomena contributed to limit the current flow, which at the light of the EIS results could be due both to an increase of  $R_{\text{ct}}$  and to a decrease of  $D_{\text{Li}}$ .

In order to study the effect of repeated cycling, two sets of EIS measurements were carried out also after 100 and 1000 cycles and are shown in Fig. 6a and b. The general trend of the Nyquist plots was again similar to what shown at the 10th charge/discharge cycle (Fig. 2a and b). However, the depression of the high frequencies loops detected in the 100 cycles spectra reflected the initial formation of surface passivating layers permeable to Li ions, also observed in preliminary Atomic Force Microscopy (AFM) ex-situ measurements. The total impedance of the cell went up with cycling as confirmed by the EIS curves recorded after 1000 cycles. A similar trend in the spectra was also observed and discussed by Aurbach et al. [16,17] in a recent work on the study of

the interactions between various electrode materials for lithium batteries and organic electrolyte solutions. The above authors demonstrated that repeated long cycle operation was related to the formation of steady surface species on the electrode. Such surface layers, permeable to Li ions, were either the product of electrolyte reduction (i.e.  $\text{ROCO}_2\text{Li}$ ; in propylene carbonate  $\text{R} = \text{CH}_3\text{CH}(\text{OCO}_2)\text{LiCH}_2-$ ) or can be formed by reprecipitation of surface species generated on surface of the Li counter-electrode, which saturate the cell solutions after long times of operation.

The impedance spectra clearly reflected the sets of time constants related to the electrical response of this surface layers that could be modeled by a 'Voight'-type element as shown in Fig. 4. Under these conditions it was not possible to calculate  $D_{\text{Li}}$  because the Warburg region could not be separated from other contributions in the spectrum. This was a special reason to use PITT measurements to calculate diffusion coefficients of aged electrodes. In Fig. 6 we reported the dependence of  $D_{\text{Li}}$  versus  $Q_{\text{ins}}$  after 10 cycles, determined by both PITT and EIS. One may observe an initial increase of  $D_{\text{Li}}$  upon  $25 \text{ mC cm}^{-2}$  of intercalated charge, followed by a decrease to  $6.2 \cdot 10^{-14} \text{ cm}^2 \text{ s}^{-1}$  when the inserted charge is  $61 \text{ mC cm}^{-2}$ . Even if the absolute values of the calculated coefficients were different both techniques agreed in giving the same trend for the diffusion coefficients upon lithium insertion. The time constants characteristic of the diffusion process, displayed in Table 1, were calculated from the frequency  $f_3$  of point L, in EIS experiments and from the limits of region III (see Fig. 5) from PITT. Not only the time constants from the two techniques showed a fair agreement, but also they seemed to have the same dependence versus injected charge. Shorter Warburg region corresponded to shorter time intervals of zone III in  $I t^{1/2}$  versus  $\log t$  plots. As shown in Fig. 7  $D_{\text{Li}}$  was calculated from PITT also at the 100th cycle at few discrete intercalation charges, multiple of  $6 \text{ mC cm}^{-2}$ . The resulting curve of  $D_{\text{Li}}$  versus  $Q_{\text{ins}}$  displayed a monotonic decay. We attributed this behavior to the increased kinetics of process A and to the vanishing of peak B already observed in the cyclic

Table 1  
Results obtained from PITT and EIS measurements

E-PITT (V)	$Q_{\text{ins-PITT}}$ ( $\text{mC cm}^{-2}$ )	$t_1$ (s)	$t_2$ (s)	$f_3^{-1}$ (s)	E-EIS (V)	$Q_{\text{ins-EIS}}$ ( $\text{mC cm}^{-2}$ )
3.2	7.1	15.5	57.3	97.1	3.2	6
2.97	12.9	6.9	17.3	39.8	2.97	12
2.77	20.5	5.6	15.25	33.3	2.77	18
2.58	24.8	5.1	13.3	27.8	2.58	24
2.45	29.7	4	12.3	19.4	2.45	30
2.13	45.0	5.4	11.4	27.8	2.2	42
1.93	55.0	10.5	22	68.0	1.95	54

$E$  indicates the potential and  $Q_{\text{ins}}$  the inserted charge;  $t_1$  and  $t_2$  are the limits of region III shown in Fig. 5;  $f_3^{-1}$  is the time constant calculated by the frequency  $f_3$  corresponding to the end point of Warburg region.

voltammograms. After 1000 cycles  $D_{Li}$  was only calculable in few potential steps and had a very low value ( $\sim 10^{-14} \text{ cm}^2 \text{ s}^{-1}$ ). Presumably the formation of a thick passivating surface layer after 1000 cycles strongly affected the current decay curve, masking the Cottrell region, similarly to what occurred in impedance spectra, where the Warburg disappeared after several cycles.

## 5. Conclusions

This work reports on a systematic study of the lithium diffusion kinetics in Ni/V mixed oxide thin films, used as transparent electrodes for ECDs. First kinetics information were obtained by CV. The CVs curves taken after 10, 100 and 1000 cycles showed two electrochemically active zones A (2.5–3.4 V) and B (1.5–2 V), probably related to two intercalation mechanisms in different hosting sites. After 10 cycles the process B was faster and peak A appeared only as a shoulder. After prolonged cycling the cathodic peak B vanished while the reaction rate around 3 V increased.

The changes of the kinetics processes observed with CV measurements were reflected in the EIS and PITT responses. After 10 charge/discharge CV cycles we calculated Li diffusion coefficients in the solid film from EIS and PITT results. Both methods were in fair agreement, giving the same non-monotonic behavior of  $D_{Li}$  as a function of the intercalation level, with a maximum around  $30 \text{ mC cm}^{-2}$  of inserted charge. We attributed this behavior to the overlapping effect of the two different diffusion processes associated with peak A and B in the CV.

Although, EIS results were of fundamental importance for understanding the physical phenomena occurring during the charge process, this technique was not suited to calculate  $D_{Li}$  after long cycling because of the presence of a passivating layer on the surface electrode. Such new layers affected the detection of the Warburg region. For this reason after 100 intercalation/deintercalation cycles the  $D_{Li}$  was measured by PITT. The trend of diffusion coefficients was a monotonic decay with values ranging from  $7.7 \times 10^{-13}$  to  $6.4 \times 10^{-14} \text{ cm}^2 \text{ s}^{-1}$ .

We can conclude, therefore, that the diffusion kinetics of lithium in Ni/V mixed oxide films is about 100 times slower than in  $\text{WO}_3$ . However, due to the high charge capacity of such Ni/V oxides, extremely thin films can be used as electrodes, offering high transparency and high cyclability without any significant capacity loss. Such films are promising candidates for applications in EC devices.

## Acknowledgements

The authors would like to acknowledge Professor C. Coluzza and Dr M. Braucci for AFM measurements.

## References

- [1] G. Inzelt, M. Pineri, J.W. Schultze, M.A. Vorotyntsev, *Electrochim. Acta* 45 (2000) 2403–2421.
- [2] C.G. Granqvist, *Handbook of Inorganic Electrochromic Materials*, Elsevier, Amsterdam 1995.
- [3] U. Opara Krasovec, B. Orel, R. Reisfeld, *Electrochem. Solid-State Lett.* 1 (1998) 104.
- [4] F. Artuso, G. Picardi, F. Decker, F. Bonino, S. Bencic, A. Surca, U. Opara Krasovec, B. Orel, *Electrochim. Acta* 46 (2001) 2077–2084.
- [5] A. Lourenco, E. Masetti, F. Decker, *Electrochim. Acta* 46 (2001) 2257–2262.
- [6] E. Masetti, F. Varsano, F. Decker, A. Krasilnikova, *Electrochim. Acta* 46 (2001) 2085–2090.
- [7] F. Varsano, F. Decker, E. Masetti, F. Croce, *Electrochim. Acta* 46 (2001) 2069–2075.
- [8] A. Surca, B. Orel, *Electrochim. Acta* 44 (1999) 3149.
- [9] C. Ho, I.D. Raistrick, R.A. Huggins, *J. Electrochem. Soc.* 127 (1980) 343–350.
- [10] J. Bisquert, G. Garcia-Belmonte, P. Bueno, E. Longo, L.O.S. Bulhoes, *J. Electroanal. Chem.* 452 (1998) 229–234.
- [11] D. Aurbach, M.D. Levi, E. Levi, H. Teller, B. Mokoovsky, G. Salitra, *J. Electrochem. Soc.* 145 (9) (1998) 3024.
- [12] M.D. Levi, D. Aurbach, *J. Phys. Chem., B* 101 (1997) 4641.
- [13] M.D. Levi, D. Aurbach, *J. Phys. Chem., B* 101 (1997) 4630.
- [14] M.D. Levi, E.A. Levi, D. Aurbach, *J. Electroanal. Chem.* 421 (1997) 89–97.
- [15] S. Lee, H.M. Cheong, C.E. Tracy, A. Mascarenhas, J.R. Pitts, G. Jorgensen, S.K. Deb, *Appl. Phys. Lett.* 76 (26) (2000) 3908.
- [16] D. Aurbach, B. Markoovsky, M.D. Levi, E. Levi, A. Schechter, M. Moshkovich, Y. Cohen, *J. Power Sources* 81–82 (1999) 95.
- [17] D. Aurbach, *J. Power Sources* 89 (2000) 206.